


Simulations of argon plasma decay in a thermionic converter

R. E. Groenewald^{✉,*}, S. Clark, A. Kannan, and P. Scherpelz[✉]
Modern Electron Inc., Bothell, Washington 98011, USA

 (Received 7 October 2020; revised 17 January 2021; accepted 31 January 2021; published 15 February 2021)

The dynamics of an argon plasma in the gap of a thermionic diode is investigated using particle-in-cell (PIC) simulations. The time-averaged diode current, as a function of the relative electrical potential between the electrodes, is studied while the plasma density depletes due to recombination on the electrode surfaces. Simulations were performed in both one and two dimensions, and significant differences were observed in the plasma decay between the two cases. Specifically, in two dimensions it was found that the electrostatic potential gradually changes as the plasma decays, while in one dimension fluctuations in the plasma led to large potential fluctuations which changed the plasma decay characteristics relative to the two-dimensional case. This creates significant differences in the time-averaged diode current. Furthermore, it was found that the maximum time-averaged current is collected when the diode voltage is set to the flat-band condition, where the cathode and anode vacuum biases are equal. This suggests a novel technique of measuring the difference in work functions between the cathode and anode in a thermionic converter.

DOI: [10.1103/PhysRevE.103.023207](https://doi.org/10.1103/PhysRevE.103.023207)

I. INTRODUCTION

Thermionic energy converters (TECs) are devices that directly convert heat into electrical energy [1,2]. The lack of moving parts and scalability (core conversion efficiency is independent of system size) of the technology makes this type of converter appealing in a wide range of applications [3]. Furthermore, thermionics are agnostic to the source of heat used, further widening its potential for impact. Examples of heat sources include solar [4], thermonuclear [5], and natural gas [6]. In its simplest form, a thermionic diode consists of two electrodes physically separated by some gap distance (referred to as the interelectrode gap). One electrode (the cathode) is heated to a temperature at which thermionic emission of electrons occur at a desired current density. The emitted current density is given by the Richardson equation, which relates the thermionically emitted current density to the electrode temperature and work function [7]. The other electrode (the anode) absorbs some of the thermionically emitted electrons. If the two electrodes are externally connected across a load, this process drives an electrical current through the circuit. Depending on the work functions of the two electrodes and the applied bias from the external circuit, the system can be either power producing or power consuming. Figure 1 shows a typical electron motive diagram of a thermionic diode. The electron motive diagram plots the negative of the electrical potential ($\phi = -eV$, where e is the electronic charge and V is electrostatic potential). The device produces power whenever the anode Fermi level is at a lower electrical potential than the cathode's, i.e., $V_{\text{out}} > 0$. The diagram also shows that as long as $V_{\text{out}} + \phi_a < \phi_c$, electrons are accelerated towards the anode, called the accelerating regime. Conversely, when $V_{\text{out}} + \phi_a > \phi_c$, electrons are decelerated as they move towards the anode, termed the retarding regime. The middle

point, when $V_{\text{out}} + \phi_a = \phi_c$, is called the flat-band condition. This corresponds to the case where V_{out} equals the contact potential difference, $\phi_c - \phi_a$.

In reality, for a vacuum thermionic diode in which the interelectrode gap is more than a few microns wide, only a small fraction of the emitted electrons make it through the gap to the anode. A space charge barrier forms in front of the cathode that reflects most of the emitted electrons back to the cathode. In such a case the diode current obeys the Child-Langmuir law [8,9]. Various strategies have been reported to increase the fraction of emitted current that makes it to the anode. Belbachir *et al.* (2014) [10] used spacers to maintain a sufficiently small interelectrode gap (10 μm) to avoid the space charge problem. Meir *et al.* (2013) [11] and Wanke *et al.* (2016) [12] used additional electrodes biased positively to reduce the space charge barrier height. Unfortunately, these methods have so far been unable to produce stable, long term operation of a thermionic converter. Another approach, used more successfully in previous TEC development programs, is to use positive ions in the gap to neutralize the space charge barrier [13,14]. Cesium plasmas have been heavily employed for this purpose since the ionization energy of cesium is low [15,16]. While these plasmas are effective at mitigating space charge, the energy required to maintain an arc discharge, defined as the arc drop, heavily reduces the efficiency of the converter [2]. This is due to the large neutral scattering cross section of cesium atoms for low energy electrons. As a solution to this problem, using inert gas plasmas has been suggested where the Ramsauer minimum makes these gases mostly transparent to low energy electrons. Using an inert gas plasma requires the plasma ignition be engineered to be very energy efficient. This can be achieved by including highly biased auxiliary electrodes that are optimally placed to produce an inert gas plasma in the gap [17,18]. Another way is to apply short high voltage pulses across a diode [19,20]. As electrons accelerate towards the anode, they collide with neutral atoms in the gap, causing ionization and eventually striking a plasma

*Corresponding author: roelof.groenewald@modernelectron.com

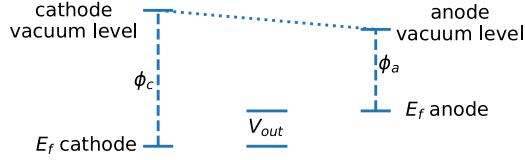


FIG. 1. Electron motive diagram to show the relation of different physical parameters of interest in a thermionic diode. E_f indicates Fermi levels, ϕ_c is the cathode work function, ϕ_a is the anode work function, and V_{out} is the output voltage of the device.

in the gap. A schematic of this is shown in Fig. 2. When the plasma producing pulse is turned off, the plasma starts to slowly decay to the electrodes (the dynamics of this decay are discussed in detail later). During this time, a large portion of the space charge cloud from thermionically emitted electrons is neutralized, and the diode current remains high. Once the plasma density has decayed to such a level that it can no longer support high diode current, the plasma ignition pulse is repeated to start the process over again. By keeping a very low duty cycle of on-to-off phases of the ignition pulse, high time-averaged diode current can be sustained with relatively little energy spent to repeatedly strike the plasma [21].

While pulsed argon plasma thermionics have been studied concerning the energy required to repeatedly strike the plasma, little is known about the impact of output voltage on the decay dynamics of the plasma, or, phrased differently, how the relative bias between the cathode and anode affects the average diode current. Understanding the IV curve of a pulsed plasma converter is important since, often, this is the only diagnostic available which researchers have to deduce several system parameters such as cathode and anode work functions, plasma density, gap, etc. In the following, this question is explored using particle-in-cell (PIC) simulations. The decay of an argon plasma in the gap of a thermionic converter as a function of time was studied with different biases applied to the anode relative to the cathode. Specifics of the simulation setup are discussed in Sec. III. It was found that the plasma lifetime is strongly dependent on the anode bias. Therefore, a characteristic of the IV curve was identified that allows extraction of the difference in electrode work functions. Fur-

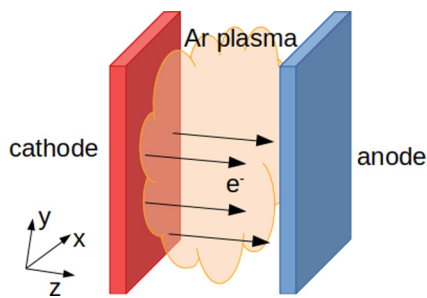


FIG. 2. Schematic of a plasma-based thermionic diode. The diode consists of two parallel plates, the cathode (left) and anode (right). Arrows indicate the direction of motion of thermionically emitted electrons as they travel from the cathode to the anode. An argon plasma is present in the interelectrode gap to neutralize the space charge formed by the emitted electrons and thereby facilitates the flow of current.

thermore, simulations were performed in both one and two dimensions, and it was found that the decay characteristics of the plasma are strongly dependent on the dimensionality of the system. Section IV describes the differences in the plasma decay under different anode biases as well as the differences that arise from dimensionality. In Sec. V the plasma sheaths are studied, and the origin of the dimensional dependence is explored.

II. THEORETICAL CONSIDERATIONS

A well-documented characteristic of pulsed inert gas plasma thermionic converters is that once the plasma producing pulse is turned off, the plasma sheath in front of the cathode rapidly inverts from an ion-accelerating to an ion-retaining (electron-rich) sheath [21,22]. This is a desirable situation since if, instead, the plasma producing pulse created a dense enough plasma to completely mitigate the thermionic space charge barrier for an extended amount of time, the decay of some number of produced ions would not affect the diode current. Therefore, the energy used to create those ions was wasted. It consequently would be more energy efficient to pulse for a shorter amount of time and instead re-pulse more frequently so that each produced ion has a maximal impact on the power producing diode current. For this reason, we can assume that during the power producing phase, the cathode sheath will always be ion retaining. According to McVey (1990) [23], the electron and ion currents can be described by the following equations:

$$J_e = \frac{2}{3} \left(J_R \exp \left[\frac{eV_c}{kT_c} \right] - J_{re} \right), \quad (1a)$$

$$J_i = (J_i/2 - J_{ri}) \exp \left[\frac{eV_c}{kT_c} \right], \quad (1b)$$

where J_R is the Richardson current emitted from the cathode, V_c is the height of the sheath in front of the cathode, T_c is the cathode temperature, and $J_{r\{i,e\}}$ are the random ion/electron currents, given by

$$J_{r\{i,e\}} = \frac{en}{4} \sqrt{\frac{8k_B T_{\{i,e\}}}{\pi M_{\{i,e\}}}}, \quad (2)$$

where e is the electron charge, n is the plasma density, T is the species temperature in the bulk plasma, k_B is Boltzmann's constant, and M is the particle mass. Notice that the same barrier, V_c , that hinders thermionically emitted electrons from entering the plasma also retains ions in the bulk plasma. This clearly indicates that achieving higher diode currents also leads to faster ion decay.

The direction of the anode sheath depends on the applied bias. Warner and Hansen (1967) [24] noted that if the anode vacuum potential is sufficiently low (compared to the cathode's), the anode sheath will be electron retaining (ion accelerating). In this configuration the ion current at the anode is simply given by $J_i = 2J_{ri}$. Seeing as the lack of an anode barrier does not increase the diode current, this configuration serves only to deplete the ion density, leading to shorter plasma lifetimes and, consequently, lower time-averaged currents. Clearly, a more favorable configuration is to also have

an ion-retaining sheath on the anode side, which, like before, gives

$$J_e = 2J_{re}, \quad (3a)$$

$$J_i = (J_i/2 + J_{ri}) \exp\left[\frac{eV_a}{kT_a}\right]. \quad (3b)$$

If we assume a perfectly neutral and uniform plasma without sheaths, an electric field will exist in the gap with $E = (V_c - V_a)/d$, where d is the interelectrode gap distance. This field vanishes when $V_c = V_a$ or, equivalently (see Fig. 9 of Ref. [13]), when $V_{\text{out}} = \phi_c - \phi_a$. Although this argument serves to form intuition, in a real system plasma sheaths will be present, and their heights will be affected by the energy distribution of the plasma particles. Seeing as the sheaths determine the plasma decay rate, correctly calculating their properties is vital to obtaining an accurate picture of the plasma decay. For this reason PIC simulations were used since the first-principles nature of these calculations provides the required accuracy for describing the plasma sheaths. The PIC simulations discussed in the following sections show that the critical point that leads to the highest time-averaged current corresponds to the flat-band condition.

The approximate plasma decay constant at flat band was derived by Rasor (1991) [13] as

$$\tau = 2\tau_i \frac{T_i}{T_c} \left[\frac{2J_s/J_0}{1 + \frac{3}{8} \frac{d}{\lambda}} \right]^{T_c/T_i}, \quad (4)$$

where τ_i is the ion crossing time, d is the gap distance, λ is the electron mean free path, J_s is the Richardson saturation current density emitted from the cathode, J_0 is the initial diode current density, T_i is the average ion temperature in the gap, and T_c is the cathode temperature. The ion crossing time $\tau_i = d/\bar{v}$ can be estimated by noting that the ion current is given by $J_i = ne\bar{v}$, where n is the plasma density and \bar{v} is the drift velocity of the ions [Eq. (2)], giving

$$\tau_i = \frac{d}{\bar{v}} = 4d \sqrt{\frac{\pi M_i}{8k_B T_i}}. \quad (5)$$

Using typical values of the diode parameters, $d = 0.5$ mm, $T_c = 1100$ °C, $T_i = 700$ °C, $d/\lambda \approx 2$, and $J_s/J_0 \approx 2$, the pulse repetition period is found to be $4\tau \approx 50$ μ s. For this reason the diode current density was averaged over a 50 μ s time interval of the plasma decay in the simulations discussed in this article.

III. METHODS

The simulations discussed in this article were performed with an adapted version of the PIC code WARP [25–27]. Specialized electrostatic field solvers were written to directly solve Poisson’s equation for the geometry of problems studied here. The one-dimensional (1D) solver uses Gaussian elimination to efficiently solve the 1D Poisson equation [28], while the two-dimensional (2D) solver uses SUPERLU [29] to decompose the finite difference matrix and quickly solve the linear system. This was found to be much faster than the multigrid solver implemented in WARP. Monte Carlo collision (MCC) handling of particle collisions [30] was added and extensively benchmarked against the results of Turner *et al.*

[31] to ensure accuracy (see the Supplemental Material [32]). The argon cross sections parameterized by Phelps [33] were used through the LXCat Phelps database, including elastic scattering processes as well as ion-neutral charge exchange. All simulations were done with a spatial resolution of 0.7 μ m. This value was chosen as it is at least 30% less than the Debye length of the densest plasma simulated, which was 1.03 μ m. The PIC time step was chosen as the maximum value such that the Courant-Friedricks-Lewey condition is still satisfied, assuming a maximum electron energy of 5 eV (much higher than the average energy simulated). This resulted in a time step of 6.15×10^{-13} s. The 1D simulations injected 10 macroparticles per time step and assumed an emission area of 1 m². The macroparticle weighting was then determined by the Richardson saturation current for the temperature conditions simulated. The 2D simulations used 24 cells in the x direction, from which 1 macroparticle was emitted per cell every time step. The y length was taken as 1 m for the calculation of the emission area and, consequently, the macroparticle weight. In one dimension (two dimensions) the initial plasma density was simulated with 1000 (100) macroparticles per cell. Particle splitting was implemented to continuously ensure sufficiently high particle count per cell during the plasma decay. The particle splitting algorithm ran every 500 simulation steps. It identified cells in which the particle count was less than 100 (10) for one dimension (two dimensions) and doubled the particle count in those cells by cloning all its particles while halving the weight. A convergence study was done to ensure simulation parameters were appropriately chosen, as shown in the Supplemental Material [32]. The simulations were performed by introducing a quasineutral plasma of a specified density between two parallel plates, as in the schematic in Fig. 2. The parallel plates are modeled as perfect conductors, thereby creating Dirichlet boundary conditions for the ends of the \hat{z} domain, and charges are absorbed when entering the conductor domains. During 2D simulations, periodic boundary conditions are used for the \hat{x} domain. The conductor plate on the left of the computational domain will be referred to as the “cathode” and is modeled as a thermionic emitter; that is, electrons are emitted from the face of the conductor. The emitted electrons have velocities sampled from the thermionic emission distribution derived in the Supplemental Material [32]. The conductor plate on the right of the computational domain will be referred to as the “anode.” In all simulations the cathode vacuum potential is used as the zero potential reference, while the anode’s vacuum potential is varied in order to study the impact of changing the output voltage of the thermionic diode. The simulations are seeded with a neutral argon plasma of specified peak density. The seeded plasma density follows a sine distribution that peaks in the middle of the gap. Simulations of plasma ignition indicate that this is close to the expected plasma density profile (see Supplemental Material [32] for further details), confirming the same result from Ref. [34]. The seed ions are assumed to be at the neutral gas temperature (for simplicity taken as the average of the cathode and anode temperatures), while the seed electrons are injected with a temperature equal to the cathode temperature, an assumption commonly made in modeling the electrons in inert-gas plasma thermionic converters (see Ref. [13], for example). This approach has two main

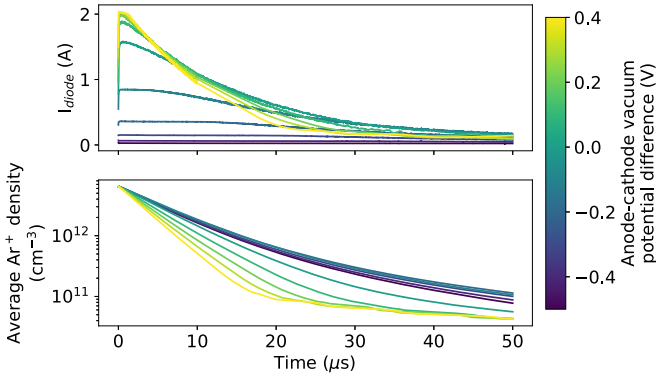


FIG. 3. Simulation results for a system with a 500 μm inter-electrode gap, 10 Torr background argon, initial plasma density of $10.2 \times 10^{12} \text{ cm}^{-3}$, and 2.2 A/cm^2 thermionic current emitted from the cathode ($T_c = 1100 \text{ }^\circ\text{C}$ and $\phi_c = 2.1 \text{ eV}$). The diode current as a function of time is shown in the top panel for different anode potentials. The average plasma density in the gap is shown in the bottom panel.

shortcomings; namely, in a real pulsed mode TEC the plasma particles would have nonzero drift velocity due to the ignition pulse, and the particle density at the electrode surfaces is not as low as predicted by the sine function. Nonetheless, this approach is used to avoid the computationally intractable problem of simulating multiple pulse periods.

The PIC simulations are evolved up to 50 μs , during which the current through the diode is continuously tracked, along with several other quantities such as the spatially resolved plasma density and electrostatic potential. Simulations were performed varying several aspects of the system, including the spacing between the electrodes, the density of the initial plasma, the current density emitted from the cathode, and the density of the background neutral gas.

IV. RESULTS

A. Two-dimensional simulations

The first set of results, shown in Fig. 3, is for a system where the interelectrode gap was set to 500 μm , the initial plasma density was set to $10.2 \times 10^{12} \text{ cm}^{-3}$, and the cathode emission current density was set to 2.2 A/cm^2 . The simulation results show that as the diode output voltage is increased, moving into the retarding regime, the diode current is suppressed. As the diode output voltage is decreased, moving into the accelerating regime, the diode current at the start of the simulation is increased, but the plasma lifetime is significantly decreased. This leads to a decrease in the diode current as the plasma density diminishes. The highest time-averaged diode current is seen when the diode is in the flat-band configuration, as shown in Fig. 4. The same simulations were done with different initial plasma densities for which the time-averaged diode current is also shown in Fig. 4. It was found in all simulated cases that the time-averaged current peaks at flat band. This same result was also seen with simulations of different gap values (250 μm and 1 mm), different background pressures (15 and 25 Torr), and other emission current densities (8.5 and 3.9 A/cm^2).

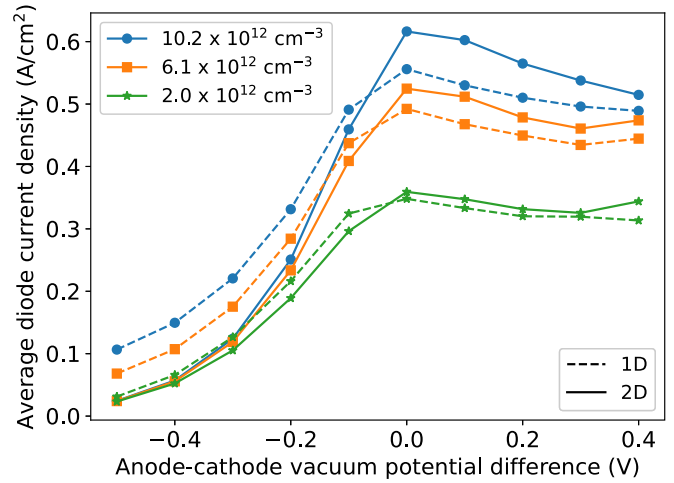


FIG. 4. Time-averaged diode current for the output voltage cases shown in Fig. 3 as well as cases with different initial plasma densities. In all three cases the time-averaged current peaks at the flat-band condition. Results for both 1D and 2D simulations are shown, highlighting the differences in simulation results.

B. One-dimensional simulations

The computational benefit of being able to do 1D simulations that accurately describe systems with translational invariance is clear. Unfortunately, it was found that the specific simulations discussed in this paper do not have the same results when performed in one dimension as in two dimensions.

As shown in Fig. 5, it was found that the plasma decay simulated in two dimensions did not match results from performing the same simulation in one dimension. Specifically, 1D simulations consistently showed faster decay of the plasma density at the beginning of the simulation compared to the 2D simulations, which then slowed down significantly as the simulation progressed. This leads to lower average current densities in the accelerating regime where the plasma density

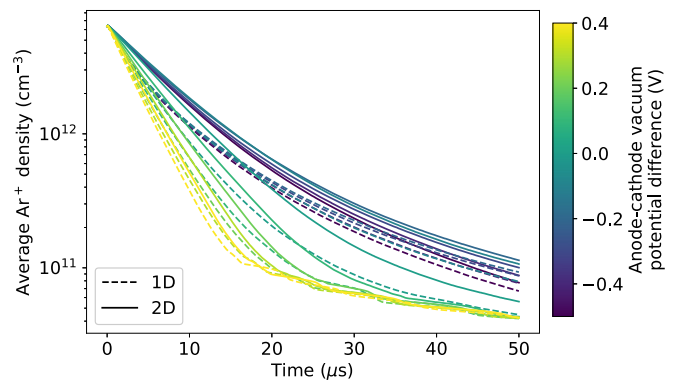


FIG. 5. Average plasma density as a function of time for different output voltages showing results from 1D (dashed) and 2D (solid) simulations. Note the differences in the plasma density between the two cases, which is the cause of the differences in time-averaged collected current. The simulation parameters were as follows: 500 μm gap, 10 Torr background argon, initial plasma density of $2.2 \times 10^{12} \text{ cm}^{-3}$, $T_c = 1100 \text{ }^\circ\text{C}$, and $\phi_c = 2.1 \text{ eV}$.

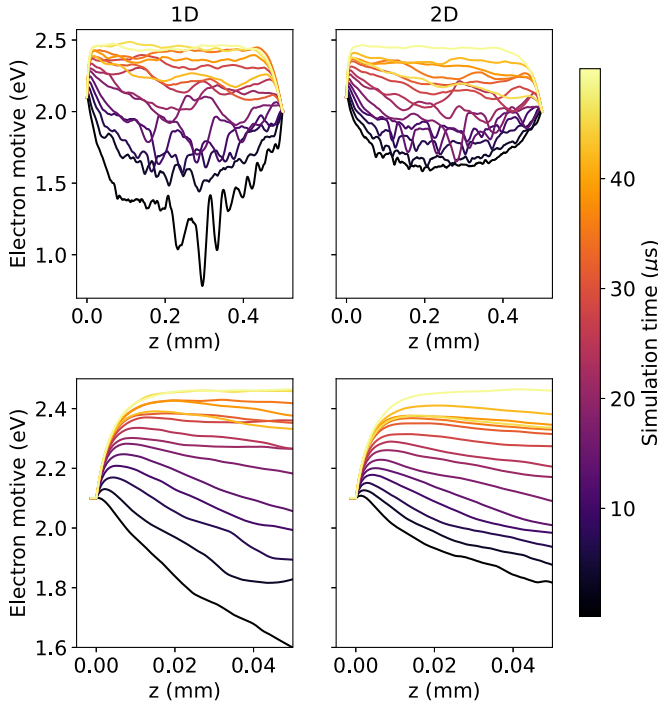


FIG. 6. Time evolution of the electron motive for both 1D and 2D simulations, over the full domain (top) and zoomed in near the cathode (bottom). The simulations are started with the same plasma density ($10.2 \times 10^{12} \text{ cm}^{-3}$), electron temperature, and ion temperature. The case shown is the one in which the anode vacuum level is biased 0.1 V relative to the cathode's.

in the early times of the simulations matters most and higher average current densities in the retarding regime where the slower decay late in the simulation matters more when compared to the 2D results (see Fig. 4).

The difference in plasma decay characteristics between the 1D and 2D simulations manifests in the electron motive evolution, as shown in Fig. 6. In two dimensions, the plasma screening is well captured, leading to relatively smooth electrostatic potential profiles throughout the plasma decay. The time-averaged rms deviation between the motive at $x = 0$ and the motive averaged over the x domain is only 61 meV, showing that small charge inhomogeneities are well screened by the surrounding plasma. In one dimension, however, the reduced dimensionality of the simulations is unable to capture the plasma screening sufficiently, leading to abrupt changes in the electrostatic potential as small regions of charge separation form. At and above flat band, these potential variations lead to a higher average barrier for beam electrons (see Fig. 6), resulting in an underprediction of the diode current compared to the 2D case. The bottom panel in Fig. 6 shows the evolution of the cathode sheath. Initially, the potential from the cathode is much steeper in one dimension than in two dimensions, which explains why the initial plasma decay is faster in one dimension than in two dimensions (ions are accelerated into the cathode with greater force in one dimension). In both 1D and 2D simulations the sheath starts out at the same potential as the cathode but quickly decreases in energy as the plasma decays and an ion-retaining sheath forms. The so-called inverse mode described by Campanell [35] is seen

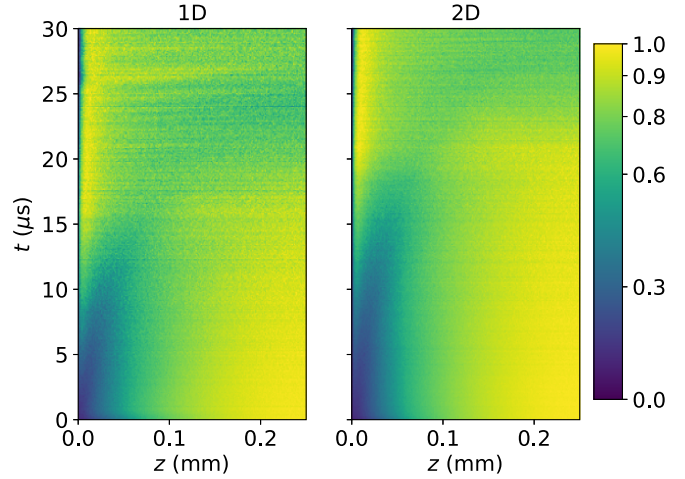


FIG. 7. Time evolution of the ion density distribution is shown for a region in front of the cathode for the same simulation case as shown in Fig. 6.

in both cases towards the end of the simulation. In Ref. [22] Campanell and Umansky argue that this state is formed due to charge-exchange collisions between ions and neutrals in the cathode sheath, trapping ions and leading to a broadening of that sheath towards the anode. Evidence of this mechanism is seen in Fig. 7, where it is clear that ion density shifts from the center of the gap to the cathode sheath. It is also notable that the 1D simulation shows a much earlier accumulation of ions in that region, which explains why the average diode current is lower for the 1D simulation in the accelerating regime.

A cut of the electron phase space (z vs v_z) is shown in Fig. 8 at different times. The phase space plots show a beam instability in both one and two dimensions. However, in two dimensions the wavelength of the beam instability increases as time progresses, indicating a damping of its growth (not seen in one dimension). This damping is due to transverse scattering of the electrons off electrostatic waves, something

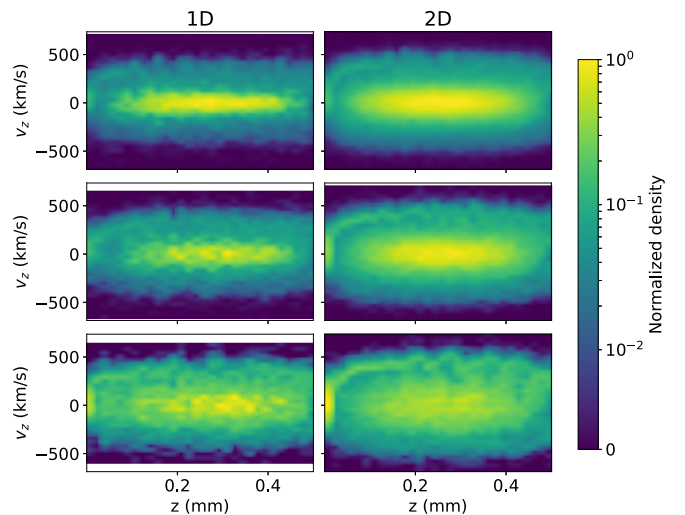


FIG. 8. Phase space plots of z versus v_z for 1D and 2D simulations at $4 \mu\text{s}$ (top), $8 \mu\text{s}$ (middle), and $12 \mu\text{s}$ (bottom) of the same simulation as shown in Fig. 6.

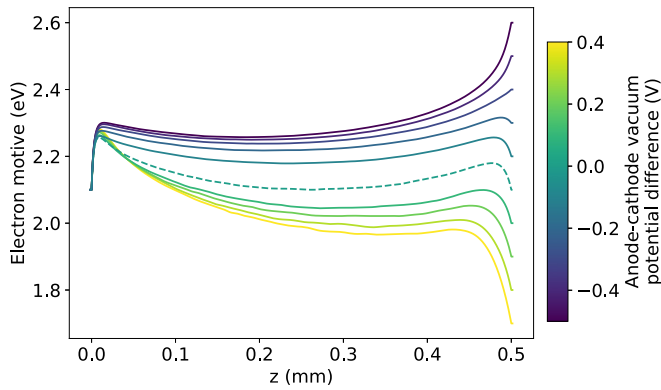


FIG. 9. The electron motive averaged over time for different anode bias cases. The flat-band condition is shown with a dashed line to highlight it. The simulation cases shown here are the same as shown in Fig. 3.

that cannot happen in one dimension since there $\vec{E} = E\hat{z}$. Evidence of this is that at $t = 12 \mu\text{s}$, the transverse temperature, $T_{\perp} = \frac{m_e}{2k_B} \langle v_{\perp}^2 \rangle$, is $2.1T_{\text{cathode}}$ in two dimensions but only $1.5T_{\text{cathode}}$ in one dimension. Greiner *et al.* [36] reported a similar formation of vortices in the electron phase space diagram of a thermionic converter. They used 1D PIC simulations to study this instability (a specific electrostatic instability known as a Pierce-Buneman instability) and observed the same undamped behavior in their 1D simulations. However, they specifically studied the plasma dynamics at high anode bias, not close to flat band. Levko [37] also showed similar beam instabilities in 1D PIC simulations of a nitrogen plasma in a thermionic converter and studied how they are affected by electron reflection from the anode.

V. DISCUSSION

The impact of diode output voltage was studied for argon plasma-based thermionic diodes. It was found that the maximum time-averaged current is collected when the diode is in the flat-band configuration. This result can be understood by studying the average electron motive for differently biased cases, as shown in Fig. 9. These results confirm the intuition discussed earlier. At highly negative biases the anode sheath becomes ion accelerating, which understandably leads to low electron current. At highly positive biases the bulk plasma potential is higher than the cathode's vacuum potential. In this condition ions from the bulk plasma easily have enough energy to overcome the ion-retaining sheaths in front of the cathode, causing fast plasma decay. Towards the flat-band condition, the sheaths in front of both electrodes become ion retaining and single valued, which is the desired condition for

slow plasma decay (as discussed earlier). The barrier index (height of cathode sheath relative to the cathode potential) is lowest exactly at flat band, which explains why the maximum time-averaged diode current is seen at flat band.

This result provides a technique to measure the difference in work functions between the cathode and anode in a thermionic converter. In practice it is difficult to determine electrode work functions in operating thermionic diodes. Typically, the work functions will be sensitive to temperature, as is the case with dispenser cathodes [38] and refractory metal electrodes that rely on cesium oxide coverage to achieve useful work functions [39]. Furthermore, evaporation and deposition of electrode material on the opposite electrode greatly alters the electrode work functions. For these reasons measurements have to be done in operating conditions to be reliable. The results discussed here indicate that an *in situ* measurement of work function differences can be done by sweeping the output voltage of an operating pulsed argon plasma diode while recording the time-averaged current. A peak in the time-averaged *IV* curve indicates the difference in electrode work functions. This in turn allows one to study more carefully the impact of changing operating conditions by tracking changes to work functions rather than solely the output power of the converter, which is a convoluted measurement of many factors. Experimental work is currently ongoing to test this proposed method.

It was also observed that simulating the plasma decay, using a PIC approach, resulted in different behavior in one dimension than in two dimensions. Specifically, higher (lower) average currents were seen in the retarding (accelerating) regime in 1D compared to 2D simulations. Therefore, in its current implementation, this type of simulation cannot be done with high fidelity in one dimension. It is believed that the dominant electron thermalization mechanism simulated is scattering off electrostatic waves, which excludes transverse scattering in the 1D case. Adding an anomalous scattering cross section in this case to enable transverse thermalization could recover fidelity in such simulations. This is left to future work. It was also noted that other authors have studied such 1D beam instabilities in similar systems using PIC codes [36,37]. Studying the dampening of these instabilities in two dimensions in further detail is also left to future work.

ACKNOWLEDGMENTS

The authors are grateful to P. Miller for his assistance in improving the parallel scaling of the internal version of WARP used for the simulations discussed in this article.

All authors contributed to the code development needed for the discussed simulations. R.E.G. ran the simulations and wrote the manuscript with input from the other authors.

- [1] G. N. Hatsopoulos and E. P. Gyftopoulos, *Thermionic Energy Conversion* (MIT Press, Cambridge, MA, 1973).
 [2] D. B. Go, J. R. Haase, J. George, J. Mannhart, R. Wanke, A. Nojeh, and R. Nemanich, *Front. Mech. Eng.* **3**, 13 (2017).

- [3] K. A. Abdul Khalid, T. J. Leong, and K. Mohamed, *IEEE Trans. Electron Devices* **63**, 2231 (2016).
 [4] P. N. Clark, in *Space Technology and Applications International Forum-STAIIF-2006; 10th Conference on Thermophysics*

- Applications in Microgravity; 23rd Symposium on Space Nuclear Power and Propulsion; 4th Conference on Human/Robotic Technology and the National Vision for Space Exploration; 4th Symposium on Space Colonization*, AIP Conf. Proc. No. 813 (AIP, Melville, NY, 2006), pp. 598–606.
- [5] E. P. Gyftopoulos and G. N. Hatsopoulos, *Electr. Eng. (Am. Inst. Electr. Eng.)* **82**, 108 (1963).
- [6] J. B. Ashton, S. E. Clark, W. Kokonaski, D. Kraemer, J. J. Lorr, M. N. Mankin, D. J. Menacher, P. D. Noble, T. S. Pan, A. De Pijper, and L. L. Wood, Combined heating and power modules and devices (2020), <https://www.freepatentsonline.com/y2020/0294779.html>.
- [7] C. Crowell, *Solid-State Electron.* **8**, 395 (1965).
- [8] C. D. Child, *Phys. Rev. (Ser. I)* **32**, 492 (1911).
- [9] I. Langmuir, *Phys. Rev.* **2**, 450 (1913).
- [10] R. Y. Belbachir, Z. An, and T. Ono, *J. Micromech. Microeng.* **24**, 085009 (2014).
- [11] S. Meir, C. Stephanos, T. H. Geballe, and J. Mannhart, *J. Renewable Sustainable Energy* **5**, 043127 (2013).
- [12] R. Wanke, G. W. J. Hassink, C. Stephanos, I. Rastegar, W. Braun, and J. Mannhart, *J. Appl. Phys.* **119**, 244507 (2016).
- [13] N. Rasor, *IEEE Trans. Plasma Sci.* **19**, 1191 (1991).
- [14] F. G. Baksht, G. A. Dyvzhev, A. M. Martsinovskiy, B. Y. Moyzhes, G. Y. Dikus, E. B. Sonin, and V. G. Yuryev, NASA, STI/Recon Technical Report N, 1978 (unpublished).
- [15] K. Hernqvist, *Proc. IEEE* **51**, 748 (1963).
- [16] D. R. Wilkins and E. P. Gyftopoulos, *J. Appl. Phys.* **37**, 2892 (1966).
- [17] P. E. Oettinger and F. N. Hussman, *IEEE Trans. Plasma Sci.* **6**, 83 (1978).
- [18] F. N. Huffman, A. H. Sommer, C. L. Balestra, D. P. Briere, and P. E. Oettinger, High efficiency thermionic converter studies, NASA Thermo Electron Corporation's Technical report TE-4233-152-77 (1976).
- [19] V. A. Zherebtsov and V. D. Talanova, *Pis'ma Zh. Tekh. Fiz.* **2**, 124 (1976).
- [20] J. McVey, in *Proceedings of the 25th Intersociety Energy Conversion Engineering Conference* (IEEE, Piscataway, NJ, 1990), Vol. 2, pp. 357–361.
- [21] Rasor Associates, Inc., Technical Report No. COO-2263-4, Office of Scientific and Technical Information (OSTI), 1975.
- [22] M. D. Campanell and M. V. Umansky, *Plasma Sources Sci. Technol.* **26**, 124002 (2017).
- [23] *Thermionic Energy Conversion: Specialist Conference Eindhoven, The Netherlands October 11-12, 1989: Proceedings*, edited by L. Wolff, W. Veltkamp, J. Schoonen, and H. Hendriksen, (Eindhoven University of Technology, Eindhoven, Netherlands 1990), pp. 71–95.
- [24] C. Warner and L. K. Hansen, *J. Appl. Phys.* **38**, 491 (1967).
- [25] See <http://warp.lbl.gov/> for code details.
- [26] A. Friedman, D. P. Grote, and I. Haber, *Phys. Fluids B* **4**, 2203 (1992).
- [27] D. P. Grote, in *Electron Cyclotron Resonance Ion Sources: 16th International Workshop on ECR Ion Sources ECRIS'04*, AIP Conf. Proc. No. 749 (AIP, Melville, NY, 2005), pp. 55–58.
- [28] C. Birdsall, *Plasma Physics via Computer Simulation* (McGraw-Hill, New York, 1985).
- [29] X. S. Li, *ACM Trans. Math. Software* **31**, 302 (2005).
- [30] C. Birdsall, *IEEE Trans. Plasma Sci.* **19**, 65 (1991).
- [31] M. M. Turner, A. Derzsi, Z. Donkó, D. Eremin, S. J. Kelly, T. Lafleur, and T. Mussenbrock, *Phys. Plasmas* **20**, 013507 (2013).
- [32] See Supplemental Material at <http://link.aps.org/supplemental/10.1103/PhysRevE.103.023207> for a derivation of the velocity distribution of thermionically emitted electrons, benchmarks of the code used in this publication and a convergence study of the results.
- [33] A. V. Phelps, *J. Appl. Phys.* **76**, 747 (1994).
- [34] J. L. Lawless and S. H. Lam, *J. Appl. Phys.* **59**, 1875 (1986).
- [35] M. D. Campanell, *Phys. Rev. E* **97**, 043207 (2018).
- [36] F. Greiner, T. Klinger, and A. Piel, *Phys. Plasmas* **2**, 1810 (1995).
- [37] D. Levko, *Phys. Plasmas* **22**, 073501 (2015).
- [38] B. Levush, Y. Lau, and K. Jensen, *IEEE Trans. Plasma Sci.* **28**, 772 (2000).
- [39] J.-L. Desplat, in *Functionally Graded Materials 1996*, edited by I. Shiota and Y. Miyamoto, (Elsevier Science B. V., Amsterdam, 1997), pp. 639–646.